# Ga–Ga bonding and tunnel framework in the new Zintl phase $Ba_3Ga_4Sb_5$

Seon-Mi Park,[a] Sung-Jin Kim,[a,1] and Mercouri G. Kanatzidis[b,*]

[a] *Department of Chemistry, Ewha Womans University, Seoul 120-750, South Korea*
[b] *Department of Chemistry and Center for Fundamental Materials Research, Michigan State University, 320 Chemistry Bldg.,*
*East Lansing, MI 48824, USA*

## Abstract

A new Zintl phase $Ba_3Ga_4Sb_5$ was obtained from the reaction of Ba and Sb in excess Ga flux at 1000°C, and its structure was determined with single-crystal X-ray diffraction methods. It crystallizes in the orthorhombic space group *Pnma* (No. 62) with $a = 13.248(3)$ Å, $b = 4.5085(9)$ Å, $c = 24.374(5)$ Å and $Z = 4$. $Ba_3Ga_4Sb_5$ has a three-dimensional $[Ga_4Sb_5]^{6-}$ framework featuring large tunnels running along the *b*-axis and accommodating the Ba ions. The structure also has small tube-like tunnels of pentagonal and rhombic cross-sections. The structure contains ethane-like dimeric $Sb_3Ga–GaSb_3$ units and $GaSb_4$ tetrahedra that are connected to form 12- and 14-membered tunnels. Band structure calculations confirm that the material is a semiconductor and indicate that the structure is stabilized by strong Ga–Ga covalent bonding interactions.
© 2003 Elsevier Inc. All rights reserved.

## 1. Introduction

Zintl phases with complex anionic frameworks and heavier elements are expected to be narrow-gap semi-conductors, and may have useful electronic properties provided they are environmentally stable. Among the pnictides, the group 13 metalates with alkaline-earth-metal cations are expected to have more extensively bonded frameworks than analogous group 14 compounds due to greater bonding requirements to fulfill the octet rule. In many ternary phases, the group 13 elements together with pnicogens atoms form tetrahedral units and their structures vary depending on how the tetrahedral units condense [1]. Recently, new air-stable anisotropic, heteroatomic Zintl frameworks, formed by group 13 and 15 elements, were found in $Ba_8In_4Sb_{16}$ [2], $RE_5In_2Sb_6$ ($RE$ = Eu, Yb) [3] and $BaGa_2Sb_2$ [4]. In $Ba_8In_4Sb_{16}$ and $Yb_5In_2Sb_6$, $InSb_4$ tetrahedra are connected by $Sb_2$ dumbbells to form covalent In/Sb frameworks. These two compounds are typical examples of group 13 antimonides, where the

more electronegative Sb atoms form homoatomic bonds or keep their lone pair electrons to achieve complete octets. However, a few related compounds show inverse behavior with homoatomic bonds found in the group 13 elements such as in $Na_2Ga_3Sb_3$ [5], $RE_{12}Ga_4Sb_{23}$ ($RE$ = La–Nd, Sm) [6] and $BaGa_2Sb_2$ [4]. $BaGa_2Sb_2$ has an interesting anionic framework with ethane-like dimeric $Sb_3Ga–GaSb_3$ units. Yet other related compounds such as $Ba_3GaSb_3$ [7], $Ba_7Ga_4Sb_9$ [8], $Sr_3GaSb_3$ [9] and $KGaSb_4$ [10] have anionic frameworks made up of only Ga-centered tetrahedral unit without homoatomic bonding. Here we describe the $Ba_3Ga_4Sb_5$ a Zintl compound with a unique framework composed of both $Sb_3Ga–GaSb_3$ and $GaSb_4$ units.

## 2. Experimental section

### 2.1. Synthesis

The crystal used in the structure determination resulted from the reaction of a mixture of three elements (Ba, Aldrich, chunk under oil, 99%; Ga, Cerac, shots, 99.999%; Sb, Cerac, chips, 99.999%) in a molar ratio 5:11:9. The excess Ga acted as flux. The reaction mixture

---

*Corresponding author. Fax: 517-353-1793.
*E-mail addresses:* sjkim@ewha.ac.kr (S.-J. Kim), kanatzid@cem.msu.edu (M.G. Kanatzidis).
[1] Also for correspondence.

was placed in a graphite tube and sealed in an evacuated silica tube. The sealed mixture was heated slowly up to 1000°C for 3 d, and kept at 500°C temperature for 3 d, and subsequently cooled to room temperature over 1 d. The reaction led to the formation of a few rod-shaped black crystals along with gray featureless pieces. Microprobe analysis on single crystals gave $Ba_{2.4(2)}Ga_{3.8(2)}Sb_{4.9(2)}$ (average of three data acquisitions). Attempts to synthesize a single phase using the correct stoichiometric ratio for $Ba_3Ga_4Sb_5$ resulted in a mixture with $BaGa_2Sb_2$.

## 2.2. Electron microscopy

Semiquantitative microprobe analysis of the compounds was performed with a JEOL JSM-35C scanning electron microscope (SEM) equipped with a Tracor Northern Energy Dispersive Spectroscopy (EDS) detector. Data were acquired using an accelerating voltage of 20 kV and a 30 s accumulation time.

## 2.3. Differential thermal analysis

Differential thermal analysis (DTA) was performed with a Labsys DTA thermal analyzer. The ground sample of manually selected single crystals of $Ba_3Ga_4Sb_5$ (∼30.0 mg total mass) was sealed in a carbon-coated silica ampoule under vacuum. A silica ampoule containing alumina of equal mass was sealed and placed on the reference side of the detector. The sample was heated to 950°C at 10°C/min and isothermed for 10 min, followed by cooling at –10°C/min to 50°C. The stability and reproducibility of the sample were monitored by running multiple heating and cooling cycles. The residue of the DTA experiment was examined with X-ray powder diffraction. The compound $Ba_3Ga_4Sb_5$ is stable at room temperature in air.

## 2.4. Electronic structure calculations

Electronic structure calculations were performed by the Hückel method within the framework of the tight-binding approximation [11]. The atomic orbital parameters employed in the calculations were default values in the CAESAR program [12,13]. Density of states (DOS) and crystal orbital overlap populations (COOP) were calculated based on 196 K point sets based on the primitive triclinic structure.

## 2.5. Crystallographic studies

A black crystal with $0.3 \times 0.3 \times 0.04 \, mm^3$ was mounted on a glass fiber. A Siemens SMART Platform CCD diffractometer was used to collect intensity data using graphite monochromatized MoKα radiation. The data were collected over a full sphere of reciprocal space

Table 1
Selected data from the single-crystal refinement of $Ba_3Ga_4Sb_5$

| Empirical formula | $Ba_3Ga_4Sb_5$ |
|---|---|
| Formula weight | 1299.65 |
| Temperature (K) | 293(2) |
| Wavelength ($\lambda = MoK\alpha$, Å) | 0.71073 |
| Crystal system | Orthorhombic |
| Space group | $Pnma$ (No. 62) |
| Unit-cell dimensions (Å) | $a = 13.248(3)$ |
| | $b = 4.5085(9)$ |
| | $c = 24.374(5)$ |
| Volume (Å$^3$) | 1455.9(5) |
| Z | 4 |
| Density, $\rho_{calc}$, (g/cm$^3$) | 5.930 |
| Absorption coefficient (mm$^{-1}$) | 24.302 |
| Reflections collected/unique | 12,826/1837 [$R_{int} = 0.044$] |
| Data/constraints/parameters | 1837/0/80 |
| Final R indices [$F_o^2 > 2\sigma(F_o^2)$]$^a$ | $R_1 = 0.0344$, w$R_2 = 0.0852$ |
| R indices ($F_o^2 > 0$) | $R_1 = 0.0357$, w$R_2 = 0.0856$ |
| Largest diff. peak and hole (e/Å$^3$) | 2.309 and −2.440 |

$^a R_1 = [\sum |F_o| - |F_c|]/\sum |F_o|$, w$R_2 = [\sum w[(F_o)^2 - (F_c)^2]^2]/[\sum w(F_o^2)^2]^{1/2}$ for $F_o^2 > 2\sigma(F_o^2)$, $w = [\sigma^2(F_o)^2 + (0.0233)P^2 + 24.6057P)]^{-1}$, where $P = (F_o^2 + 2F_c^2)/3$.

Table 2
Atomic coordinates ($\times 10^4$) and equivalent isotropic displacement parameters (Å$^2 \times 10^3$) for $Ba_3Ga_4Sb_5$

| Atom | Wyckoff position | $x$ | $y$ | $z$ | Occupancy (%) | $U_{eq}{}^a$ |
|---|---|---|---|---|---|---|
| Ba(1) | 4c | 1431(1) | 1/4 | 7202(1) | 100 | 18(1) |
| Ba(2) | 4c | 9834(1) | 3/4 | 8852(1) | 100 | 25(1) |
| Ba(3) | 4c | 1718(1) | 1/4 | 5044(1) | 100 | 23(1) |
| Sb(1) | 4c | 2044(1) | 3/4 | 6129(1) | 100 | 13(1) |
| Sb(2) | 4c | 4110(1) | 1/4 | 7146(1) | 100 | 13(1) |
| Sb(3) | 4c | 2221(1) | 3/4 | 8235(1) | 100 | 14(1) |
| Sb(4) | 4c | 9439(1) | 1/4 | 5848(1) | 100 | 18(1) |
| Sb(5) | 4c | 1202(1) | 1/4 | 9708(1) | 100 | 13(1) |
| Ga(1) | 4c | 70(1) | 3/4 | 6355(1) | 100 | 16(1) |
| Ga(2) | 4c | 9053(1) | 3/4 | 7235(1) | 100 | 14(1) |
| Ga(3) | 4c | 2484(1) | 1/4 | 8839(1) | 100 | 16(1) |
| Ga(4) | 4c | 901(2) | 3/4 | 253(1) | 50 | 11(1) |
| Ga(5) | 4c | 3033(2) | 1/4 | 6172(1) | 50 | 10(1) |

$^a U_{eq}$ is defined as one-third of the trace of the orthogonalized $U_{ij}$ tensor.

up to 56° in 2θ. The individual frames were measured with an ω rotation of 0.3° and an acquisition time 30 s. To check the stability of the crystal, at the end of data collection procedure the initial 50 frames of data were measured again and compared. No crystal decay was detected. The SMART software [14] was used for data acquisition and SAINT for data extraction and reduction. The absorption correction was performed empirically using SADABS. The unit cell parameters were obtained from the least-squares refinement of 600 randomly chosen reflections, from a full reciprocal sphere of data up to 56° in 2θ, see Table 1. The observed Laue symmetry and systematic extinctions were indicative of the space groups $Pnma$ or $Pn2_1a$. The
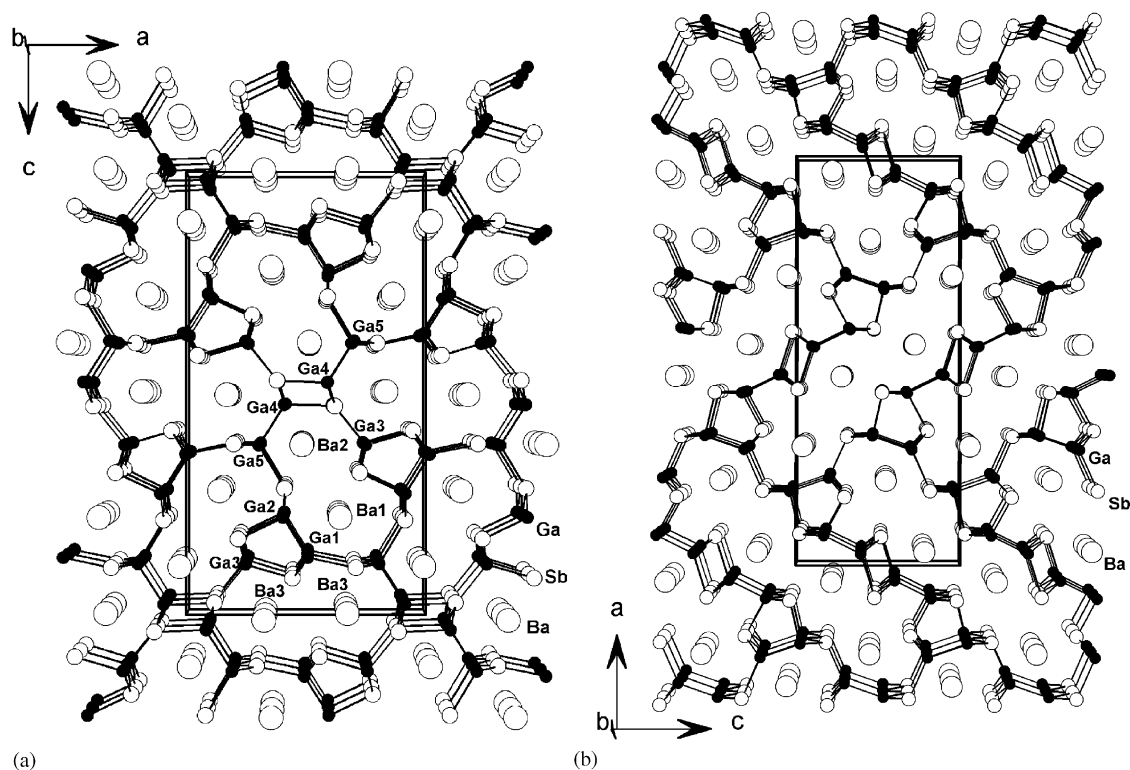
Fig. 1. (a) A [010] view of the orthorhombic unit cell of $Ba_3Ga_4Sb_5$. (b) A [010] view of the orthorhombic unit cell of $BaGa_2Sb_2$. The Sb, Ga, and Ba atoms are indicated small open, small filled, and large open circles, respectively.

centrosymmetric *Pnma* was assumed, and subsequent refinements confirmed the choice of this space group. The initial positions of all atoms were obtained from direct methods of the SHELXS-97 program. The structure was refined by full-matrix least-squares techniques with the use of the SHELXL-97 program package of crystallographic program. Once all atoms were located, the thermal parameters of Ga(4) and Ga(5) were abnormally higher values suggesting partial occupancies. When the occupancies of Ga(4) and Ga(5) atoms were allowed to vary, the refinements led to 48(3)% and 50(3)% occupation factor, respectively. Subsequently, the occupancies of Ga(4) and Ga(5) atoms were fixed to 50%. The final cycle of refinement was performed on $F_o^2$ with 80 variables and 1837 averaged reflections. The complete data collection parameters and details of structure solution and refinement are given in Table 1. Final atomic positions and isotropic displacement parameters are given in Table 2.

## 3. Results and discussion

The compound $Ba_3Ga_4Sb_5$ adopts a new structure type. It features a $[Ga_4Sb_5]^{6-}$ framework with large tunnels running along the [010] direction. $Ba^{2+}$ cations reside in straight tunnels made from 12- and 14-membered rings (Fig. 1a). The 12-membered ring contains Ba(1) and Ba(2), and 14-membered ring contains two Ba(3). The basic building blocks of the anionic network $[Ga_4Sb_5]^{6-}$ units are Ga–Ga dimers (two types) with an ethane like staggered conformation and GaSb$_4$ tetrahedra. The dimers and tetrahedra share Sb atoms to form tubes with small 4- and 5-membered ring cross-sections. To our knowledge, compounds with the ethane like $Ga_2Sb_6$ units are rare with $BaGa_2Sb_2$ and $Na_2[Ga_3Sb_3]$ being the only prior examples [4,5]. The overall structure of $Ba_3Ga_4Sb_5$ is similar to that of $BaGa_2Sb_2$, where also ethane-like Ga–Ga dimers are found as seen in the comparison shown in Fig. 1. However, $Ba_3Ga_4Sb_5$ also contains GaSb$_4$ tetrahedral units. Furthermore one out of two Ga–Ga dimer sites, Ga(4)–Ga(5), is empty. The structural refinements show that the Ga(1)–Ga(2) sites are fully occupied and Ga(4)–Ga(5) sites are exactly 50% occupied indicating the possibility of a superstructure (Fig. 2).[2]

The Ga–Ga bond lengths in the two crystallographically distinct fragments Ga(1)–Ga(2) and Ga(4)–Ga(5) are 2.533(2) and 2.647(3) Å, respectively. These bond

---

[2] The zone photographs taken with long exposure time (1200 s per frame) at 173 K gave evidence of superstructure with doubling of the *b*- and *c*-unit cell parameters. However, the intensities of the superstructure reflections were too weak to resolve and refine the ordered structure.
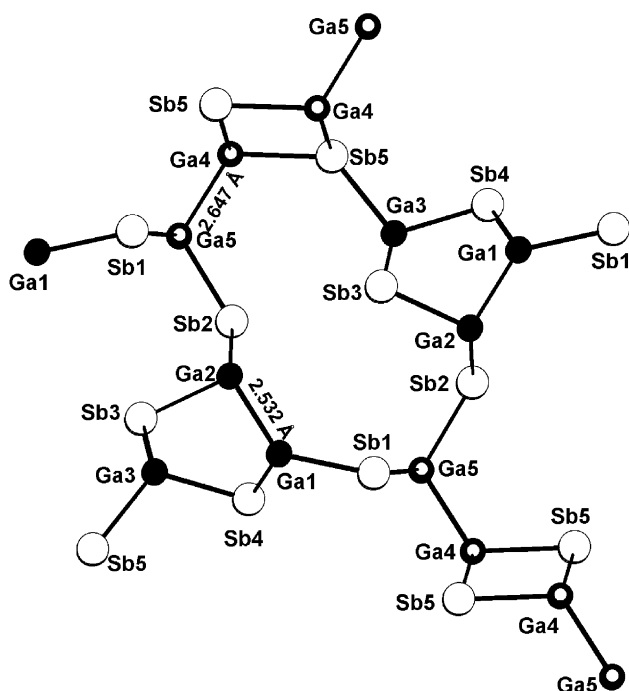
Fig. 2. Detailed view of a fragment of the $[Ga_4Sb_5]^{6-}$ framework with atomic labeling. The partially occupied Ga(4) and Ga(5) atoms are indicated small filled and thick-lined open circles, respectively. The Sb atoms are indicated small open circles.

Table 3
Selected bond distances (Å) and angles (deg) in $Ba_3Ga_4Sb_5$

| | | | |
|---|---|---|---|
| Ga(1)–Ga(2) | 2.5330(19) | Ba(3)–Ga(3)(×2) | 3.8510(14) |
| Ga(4)–Ga(5) | 2.647(3) | Ba(3)–Sb(4)(×2) | 3.4872(10) |
| Ga(1)–Sb(4) | 2.7032(10) | Ba(3)–Sb(1)(×2) | 3.5003(10) |
| Ga(2)–Sb(2)(×2) | 2.7147(9) | Ba(3)–Sb(4) | 3.5993(13) |
| Ga(3)–Sb(4) | 2.7003(18) | Ba(3)–Sb(5) | 3.6527(10) |
| Ga(3)–Sb(3) | 2.7145(10) | — | — |
| Ga(4)–Sb(5) | 2.6471(14) | Ga(2)–Ga(1)–Sb(1) | 134.05(6) |
| Ga(4)–Sb(5) | 2.788(3) | Ga(2)–Ga(1)–Sb(4) | 102.86(4) |
| Ga(5)–Sb(1) | 2.6092(13) | Sb(1)–Ga(1)–Sb(4) | 102.02(4) |
| Ba(1)–Ga(5) | 3.287(3) | Sb(4)–Ga(1)–Sb(4) | 113.01(6) |
| Ba(1)–Ga(1)(×2) | 3.5497(12) | Ga(1)–Ga(2)–Sb(3) | 96.89(6) |
| Ba(1)–Ga(2)(×2) | 3.8755(14) | Ga(1)–Ga(2)–Sb(2) | 117.16(3) |
| Ba(1)–Sb(2) | 3.4628(12) | Sb(3)–Ga(2)–Sb(2) | 105.22(4) |
| Ba(1)–Sb(2) | 3.5507(13) | Sb(2)–Ga(2)–Sb(2) | 112.28(6) |
| Ba(1)–Sb(3)(×2) | 3.5377(10) | Sb(4)–Ga(3)–Sb(3) | 106.07(4) |
| Ba(1)–Sb(1)(×2) | 3.5479(10) | Sb(3)–Ga(3)–Sb(3) | 112.29(6) |
| Ba(2)–Ga(4)(×2) | 3.2836(19) | Sb(4)–Ga(3)–Sb(5) | 112.28(6) |
| Ba(2)–Ga(4) | 3.697(3) | Sb(3)–Ga(3)–Sb(5) | 110.03(4) |
| Ba(2)–Ga(5)(×2) | 3.2829(19) | Sb(5)–Ga(4)–Sb(5) | 110.14(6) |
| Ba(2)–Sb(2)(×2) | 3.4520(9) | Sb(5)–Ga(4)–Sb(5) | 116.77(10) |
| Ba(2)–Sb(3) | 3.5016(13) | Ga(5)–Ga(4)–Sb(5) | 120.32(11) |
| Ba(2)–Sb(5)(×2) | 3.5666(9) | Sb(5)–Ga(4)–Sb(5) | 99.64(6) |
| Ba(2)–Sb(1) | 3.6957(13) | Sb(1)–Ga(5)–Sb(1) | 119.53(10) |
| Ba(2)–Sb(5) | 3.7680(13) | Sb(1)–Ga(5)–Ga(4) | 103.50(7) |
| Ba(3)–Ga(4) | 3.194(3) | Sb(1)–Ga(5)–Sb(2) | 107.06(6) |
| Ba(3)–Ga(5) | 3.254(3) | Ga(4)–Ga(5)–Sb(2) | 116.75(10) |

lengths are comparable to the sum of covalent radii (2.52 Å) and also comparable to those found in $BaGa_2Sb_2$, $Na_2[Ga_3Sb_3]$ and $Pr_{12}Ga_4Sb_{23}$. In $Ba_3Ga_4Sb_5$ the tetrahedral angles around the Ga atoms are in a range of 96.89(6)–134.05(6)° for the dimers and 106.07(4)–112.29(6)° for the single $GaSb_4$ tetrahedra (Table 3). The local geometry around Ga in the tetrahedral $GaSb_4$ is close to the ideal tetrahedral bond angle. This indicates that the geometry around the Ga–Ga dimers is more flexible and responds to the size of electropositive cations filling the framework. The Ga–Sb bond distances are in the range 2.610(1)–2.788(3) Å in $Ba_3Ga_4Sb_5$, in accordance with normal covalent bonding and comparable to that in $BaGa_2Sb_2$ at 2.665(1)–2.817(1) Å.

The $Ba^{2+}$ ions are surrounded by six or seven Sb atoms with additional Ga atoms at a longer distance, Fig. 3. The Ba(1) atoms are in capped trigonal prismatic geometry if we consider only the nearest six Sb atoms at 3.463(1)–3.551(1) Å and one Ga atom at 3.287(3) Å as real bonds. The next nearest distances of 3.550(1) and 3.875(1) Å to Ga(1) and Ga(2) atoms are probably too long to be considered bonds.[3] The Ba(2) atoms are first surrounded by six Sb atoms at 3.452(1)–3.696(1) Å and two Ga atoms at 3.283(2) Å, and all eight atoms define a bicapped trigonal prism geometry. The next neighbors

are the Sb(5) and Ga(4) atoms at distances 3.768(1) and 3.697(3) Å, too long to be considered as bonds. The Ba(3) atoms are first surrounded by seven Sb atoms at 3.487(1)–3.653(1) Å and two Ga atoms at 3.194(3) and 3.254(3) Å, and all define a tricapped trigonal prismatic geometry.

If we assume the oxidation state of Sb atoms to be −3, that of Ga in the $GaSb_4$ unit +3, and the Ga atoms in the ethane like Ga(1)–Ga(2) and 50% occupied Ga(4)–Ga(5) dimers to be in $(Ga_2)^{4+}$ units, then the formula can be represented as $(Ba^{2+})_3[(Ga^{3+})(Ga_2^{4+}) (Ga_2^{4+})_{0.5}(Sb^{3-})_5]^{6-}$. Alternatively, if we consider that only every other Ga(4)–Ga(5) dimer is there, then electron counting leads to the formulation $(Ba^{2+})_3[(4bGa^{1-})_3(3bSb^0)_2\{(Ga^{1-})_2(3bSb^0)_2(4bSb^{1+})\}_{0.5} \{\bullet_2(1bSb^{2-})_2(2bSb^{1-})\}_{0.5}]^{6-}$, where $\{(Ga^{1-})_2(3bSb^0)_2 (4bSb^{1+})\}_{0.5}$ represents electron counting for when the Ga–Ga dimers are there, and $\{\bullet_2(1bSb^{2-})_2(2bSb^{1-})\}_{0.5}$ represents the case when the Ga–Ga dimers are absent. Both of these representations achieve valence precision and are also consistent with the Zintl concept.

### 3.1. Thermal analysis

The compound $Ba_3Ga_4Sb_5$ is stable at room temperature in air. DTA shows the compound congruently melts at 714°C and crystallizes at 658°C. The melting and crystallization temperature of $Ba_3Ga_4Sb_5$ are

---

[3] The single bond distances of Ba–Sb and Ba–Ga calculated from metallic radii are 3.606 and 3.461 Å, respectively.

*Represents a vacancy.
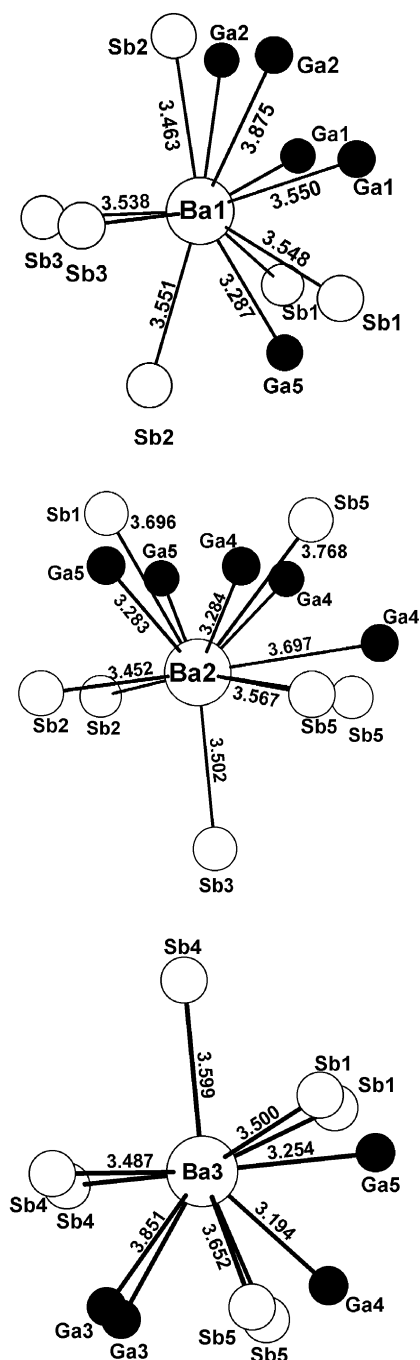
Fig. 3. Coordination environment of the three crystallographically different Ba atoms in $Ba_3Ga_4Sb_5$.

similar to those of $BaGa_2Sb_2$ at 767°C and 666°C, respectively.

### 3.2. Electronic structure

To gain additional insight into the chemical bonding in this material, band structure calculations were performed on the anionic $[Ga_4Sb_5]^{6-}$ framework, using a hypothetically ordered triclinic superstructure with



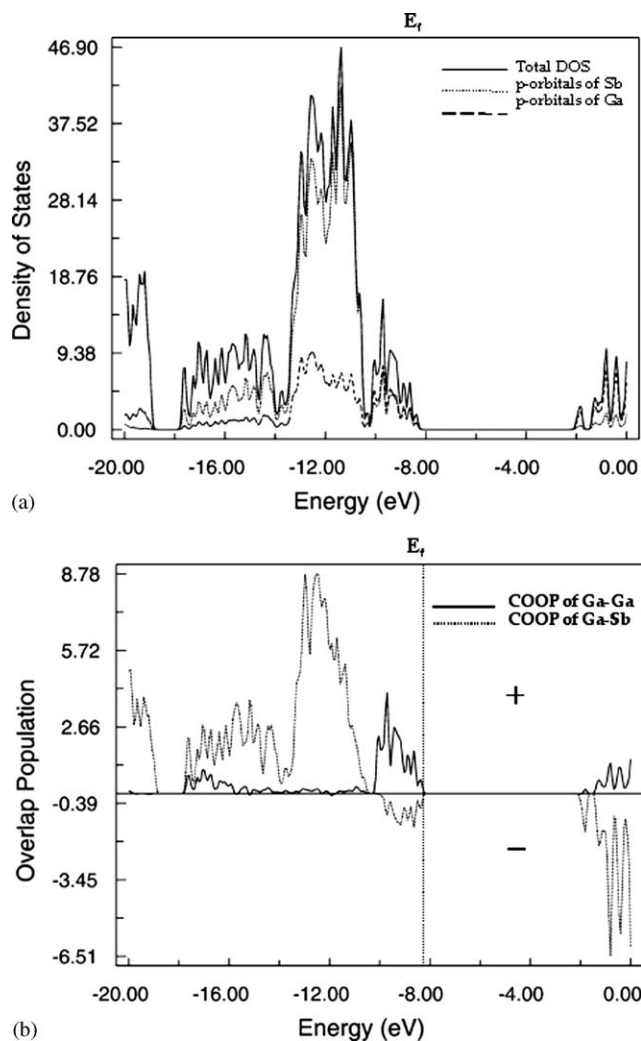Fig. 4. COOP and DOS curves for $Ba_3Ga_4Sb_5$. (a) Total DOS and projected DOS curves. The projection of Ga 4p (dash–dotted line), Sb 5p (dotted line), and total DOS (solid line) curves are shown. (b) COOP curves of Ga–Ga (solid line) and Ga–Sb (dotted line) interaction indicate that structure is stabilized by covalent Ga–Ga interactions. The bonding and antibonding characters are illustrated as positive and negative overlap populations.

alternatingly filled Ga(4)–Ga(5) dimers.[4] The band structure was calculated using the extended-Hückel formalism with the atomic orbital parameters use previously for $BaGa_2Sb_2$. DOS and COOP were calculated based on 196 K points, and the results are shown in Fig. 4. The band structure calculations also support $Ba_3Ga_4Sb_5$ to be structurally and electronically a Zintl phase. The calculations show that the valence states are completely filled and the Fermi level occurs just below the energy gap suggesting a

---

[4] The results of band calculation using other hypothetically ordered orthorhombic Superstructure models with respect to the Ga(4)–Ga(5) dimers also showed similar features with completely filled valence band.

semiconductor. The detailed energy dispersion analysis between several high symmetry points in the first Brillouin zone suggests the energy gap is direct. The band gap was not measurable experimentally due to being very narrow ($<0.12$ eV) and beyond the reach of our instrumentation.

The DOS plot in Fig. 4(a) contains total densities together with projections for the Ga $p$ and Sb $p$ orbital contributions. The valence band is relatively wide at about 9.5 eV, which is due to the strong, three-dimensionally extended Ga–Sb interactions. The projected DOS shows that the states near $E_f$ are mainly contributions from Ga $4p$ and Sb $5p$ orbitals mixed with some corresponding $s$ orbital character. The block of states at lower energy ($<-10$ eV) are dominated by $p$ orbitals of Sb and the states above $-10$ eV are dominated by $p$ orbitals of Ga. This is consistent with their electronegativity difference.

In COOP plots, the projections for Ga–Ga and Ga–Sb bonds are shown in Fig. 4(b). The states just below $E_f$ are mainly from Ga–Ga bonding interactions, which suggests that the strong covalent Ga–Ga bonding is significantly contributing to the stability of the compounds. Just below the Fermi level there exist some antibonding Ga–Sb states suggesting some weakening of bonding interactions in Ga–Sb.

## Acknowledgments

## Supporting information

Further details of the crystal structure investigation(s) can be obtained from the Fachinformationszentrum Karlsruhe, 76344 Eggenstein-Leopoldshafen, Germany (fax: (49) 7247-808-666; e-mail: crysdata@fiz.karlsruhe.de); The depository number for $Ba_3Ga_4Sb_5$ compound is CSD 413032.

## References

[1] S.M. Kauzlarich, Chemistry, Structure, and Bonding of Zintl Phases and Ions, VCH Publishers, New York, 1996.
[2] S.-J. Kim, S. Hu, C. Uher, M.G. Kanatzidis, Chem. Mater. 11 (1999) 3154.
[3] (a) S.-J. Kim, J. Ireland, C.R. Kannewurf, M.G. Kanatzidis, J. Solid State Chem. 155 (2000) 55;
    (b) S.-M. Park, E.-S. Choi, W. Kang, S.-J. Kim, J. Mater Chem. 12 (2002) 1839.
[4] S.-J. Kim, M.G. Kanatzidis, Inorg. Chem. 40 (2001) 3781.
[5] G. Cordier, H. Ochmann, H. Schäfer, Mater. Res. Bull. 21 (1986) 331.
[6] A.M. Mills, A. Mar, Inorg. Chem. 39 (2000) 4599.
[7] G.H. Cordier, H. Schäfer, M.Z. Stelter, Naturforscher 40B (1985) 1100.
[8] G.H. Cordier, H. Schäfer, M.Z. Stelter, Anorg. Allg. Chem. 534 (1986) 137.
[9] G.H. Cordier, H. Schäfer, M.Z. Stelter, Naturforsch 42B (1987) 1268.
[10] G. Cordier, H.Z. Ochmann, Kristallografiya 195 (1991) 306.
[11] (a) R.J. Hoffman, Chem. Phys. 39 (1963) 1397;
     (b) E. Canadell, M.-H. Whangbo, Chem. Rev. 91 (1991) 965.
[12] (a) M. Wolfsberg, L.J. Helmholz, Chem. Phys. 20 (1952) 837;
     (b) C.J. Ballhausen, H.B. Gray, Molecular Orbital Theory, Benjamin, New York, 1965;
     (c) H. Basch, A. Viste, H. Gray, Theoret. Chim. Acta 3 (1965) 458;
     (d) H. Basch, A. Viste, H.J. Gray, Chem. Phys. 44 (1966) 10;
     (e) V. Baranovskii, A. Nikolskii, Theor. Eskp. Khim. 3 (1967) 527.
[13] J. Ren, W. Liang, M.-H. Whangbo, CAESAR 1.0 Primecolor Software, Inc., Cary, North Carolina, 1998.
[14] (a) SMART, Siemens Analytical X-ray Systems, Inc., Madison, WI, 1994;
     (b) SAINT, Siemens Analytical X-Ray Systems, Inc., Madison, WI, 1995.